Design and Optimization Procedure of a Single-Sided Linear Induction Motor Applied to an Articulated Funiculator

Yifei Hu[1], Alija Cosic[2], Stefan Östlund[1], and Hui Zhang[1]
[1]Department of Electric Power and Energy Systems, KTH-Royal Institute of Technology, Stockholm, Sweden
[2]Department of Electric Power, Swedish Transport Administration, Stockholm, Sweden
Email: yifeih@kth.se

***Abstract*—The paper describes the design of a single-sided linear induction motor (SLIM) intended for an Articulated Funiculator (AF). A procedure is proposed where first an analytical design is carried out to obtain a preliminary geometry. The analytical design is based on approximate equivalent circuits under constrained conditions. In the second step a two-dimensional finite element method (2D-FEM) analysis is performed to validate the accuracy of the analytical models. The modification and optimization are conducted to acquire the best design.**

Keywords—analytical model; single-sided linear induction motor; finite element method; optimization.

I. INTRODUCTION

As a part of the group of special electrical machines, linear induction motors (LIMs) convert electrical energy directly into mechanical energy by means of translatory motion [1]. In principle, for every rotary electric machine, there exists a linear motion counterpart [2]. Therefore, a LIM is generally described as an unfolded rotary electric machine and they have the same working principle. The exciting part of the LIM, in analogy to the stator in the traditional rotary machine, is called the primary, while the other part in which currents are induced similar to the rotor in the traditional rotary induction machine is called the secondary of the LIM [3]. Compared to rotary induction machines, LIMs have the merits of simple construction, direct electromagnetic thrust propulsion, safety and reliability, and precise linear positioning [2]. As a result of these advantages, LIMs have a variety of applications such as transportation, actuators, pumps and elevators [4].

Aiming at a new and innovative solution to vertical transportation, the Articulated Funiculator (AF), shown in Fig. 1, is developed by Tyréns AB as a continuous and connected system of pods that moves passengers in masse. An idea of "sky subway" is to be achieved, which means the pods lie horizontal at specific floor levels designated as "stations" and vertical alignments between stations, forming a complete loop transition. In this way, the AF demands only two vertical shafts, largely decreasing the amount of elevators and increasing the rentable/sellable floor space percentage compared to conventional elevator systems. [5]

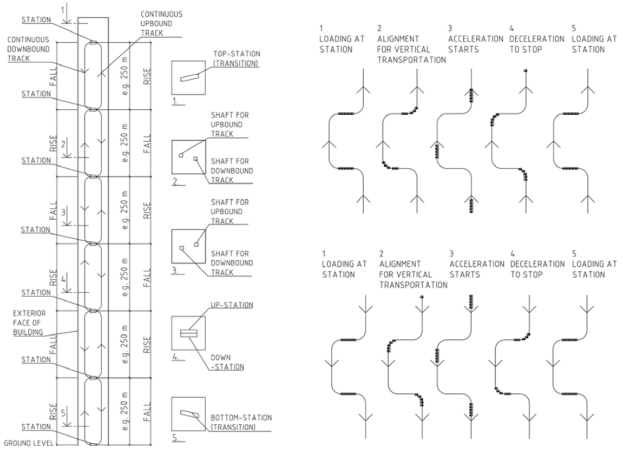

Fig. 1: Articulated funiculator concept sketches [5].

Having the simplest construction and best structural compatibility with the pods of the AF, single-sided linear induction motors (SLIMs) are considered to be a feasible solution to the propulsion system of the AF. Additionally, the required velocity is 10 m/s, which is regarded as low for LIMs, and thereby the dynamic end effect of LIMs is not significant. In order to accelerate the pods upwards with up to 2 m/s^2, applying several primary units in parallel to jointly propel a single pod, is a more effective scheme.

II. ANALYTICAL MODEL DESIGN

In order to obtain the preliminary geometry and analyze the steady-state performance of the LIM, an analytical model is first designed based on the following objectives: the thrust produced by the collection of SLIMs F_t is no less than the total required force to move the system F_s'; the maximum value of the normal component of the flux density in the air gap B_{gmax} is supposed to be slightly less than 0.6 T. For the purpose of reducing normal attractive force as well as the magnetizing current, low values of B_{gmax} for large SLIMs are preferred [1]. According to [6], the iron losses of a SLIM are negligible when B_{gmax} is below 0.5 T. For large motors, the attractive force can be reduced by keeping B_{gmax} below 0.6 T [1]. Nevertheless, B_{gmax} is also determining the useful thrust, which results in the trade off between the iron losses and thrust on one hand, the

978-1-5090-1210-7/16/$31.00 ©2016 IEEE

attractive force and thrust on the other hand. Here B_{gmax} of large LIMs, therefore, is designed to be slightly less than 0.6 T. Additionally, no iron saturation of any part of the designed SLIMs is allowed. Moreover, the size of the collection of the SLIMs should be designed within the scope of the pod.

A. Approximate equivalent circuit

A single-phase approximate equivalent circuit, as shown in Fig. 2, is employed to acquire the characteristics of the SLIMs. Per-phase primary winding resistance R_1 is expressed in (1) where ρ_w is the volume resistivity of copper, l_w is the length of copper wire in one phase, and A_w is the cross-sectional area of that. Per-phase primary leakage reactance X_1 can be approximately calculated by (2) [7] where μ_0, f, λ_s, λ_d, W_s, q_1, λ_e, l_{ce}, N_1, and p correspond to the permeability of free space, input frequency, slot leakage permeance coefficient, specific permeance between the heads of teeth, primary core width, number of slots per pole per phase, end-connection leakage permeance coefficient, length of end winding, number of turns per phase, and number of poles. The expression of magnetizing reactance X_m is given in (3) [7] where W_{se}, k_w, τ, and g_e indicate the equivalent width of primary core, winding factor, pole pitch, and equivalent length of air gap due to slotted structure. Per-phase secondary resistance R_2 is obtained in (4) where G is the goodness factor.

$$R_1 = \rho_w \frac{l_w}{A_w} \tag{1}$$

$$X_1 \cong \frac{8\mu_0 \pi f \left[(\lambda_s + \lambda_d)\frac{W_s}{q_1} + \lambda_e l_{ce}\right] N_1^2}{p} \tag{2}$$

$$X_m \cong \frac{24\mu_0 f W_{se}(k_w N_1)^2 \tau}{\pi p g_e} \tag{3}$$

$$R_2 = \frac{X_m}{G} \tag{4}$$

B. Steady-state characteristics

After having derived the parameters of the equivalent circuit, the steady-state characteristics may be expressed by starting with the input power factor $\cos\phi$, where ϕ is the phase angle of the total impedance of single-phase equivalent circuit. The thrust produced by each SLIM unit F_s is given by

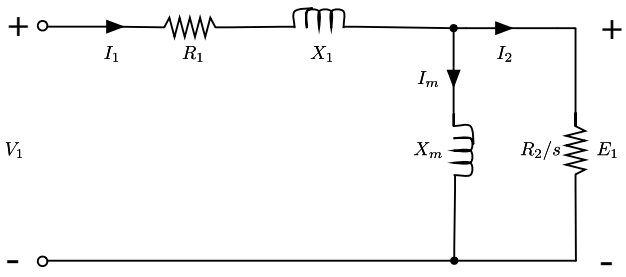

Fig. 2: Single-phase approximate equivalent circuit.

$$F_s = \frac{mV_1 I_1 \cos\phi - mI_1^2 R_1 - mI_2^2 R_2}{v_r} \tag{5}$$

Where m is the number of phases, V_1 is the input phase voltage, I_1 is the primary phase current, I_2 is the secondary phase current, and v_r is the linear motion velocity. The efficiency η is shown as

$$\eta = \frac{F_s v_r}{mV_1 I_1 \cos\phi} \tag{6}$$

The peak value of the normal component of the magnetic flux density in the air gap B_{gmax} is expressed as [1]

$$B_{gmax} = \frac{\mu_0 \Theta_m}{2g_e} \tag{7}$$

Note that Θ_m is the resulting magnetomotive force (MMF) of m phases, given by [1]

$$\Theta_m = \frac{4\sqrt{2} m k_w N_1 I_m}{\pi p} \tag{8}$$

Where I_m is the magnetizing current. The force required to be produced by the propulsion system F_s' is derived from

$$F_s' = m_t(a + g) + D \tag{9}$$

Where m_t is the mass of the entire moving system including that of passengers, pod and applied primary units since they are attached to the pod moving along with them, a and g are the rising and gravitational acceleration, respectively, D is the total resistance composed of aerodynamic and rolling resistance. The total thrust produced by number of n_{pri} SLIM units F_t is given by

$$F_t = n_{pri} F_s \tag{10}$$

C. Design procedures and analytical results

For a more intuitive understanding, the analytical model design procedures are illustrated with the flow charts shown in Figs. 3 and 4, where N_c is the number of turns per slot, b indicates the slot width to pitch ratio, and s_{rated} is the rated slip. The design procedures are programed with MATLAB that can lead to a digital implementation. Based on the design algorithm, the 8-pole and 6-pole SLIM can be modeled.

The analytical results are shown in Figs. 5-8. The geometry with the primary core, aluminum sheet, and back iron included of the analytically designed 8-pole and 6-pole SLIM is shown in Figs. 5 and 7, respectively, where the unit is meter (the scale for the horizontal and vertical axis is different). Fig. 6 indicates that the 8-pole SLIM is operating at the rated slip of 0.06, producing a thrust of 1.052e+04 N. The pull-out thrust is 2.183e+04 N at the slip of 0.23. Nevertheless, the machine is not tolerated to be working at the slip with respect to pull-out torque/thrust for a stable performance. The similar information of the 6-pole SLIM can be obtained from Fig. 8.

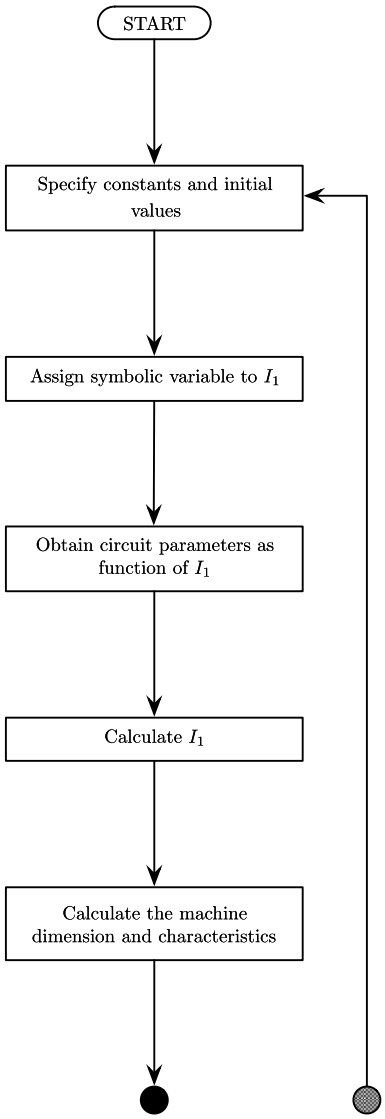

Fig. 3: Flow chart of analytical design, part 1/2.

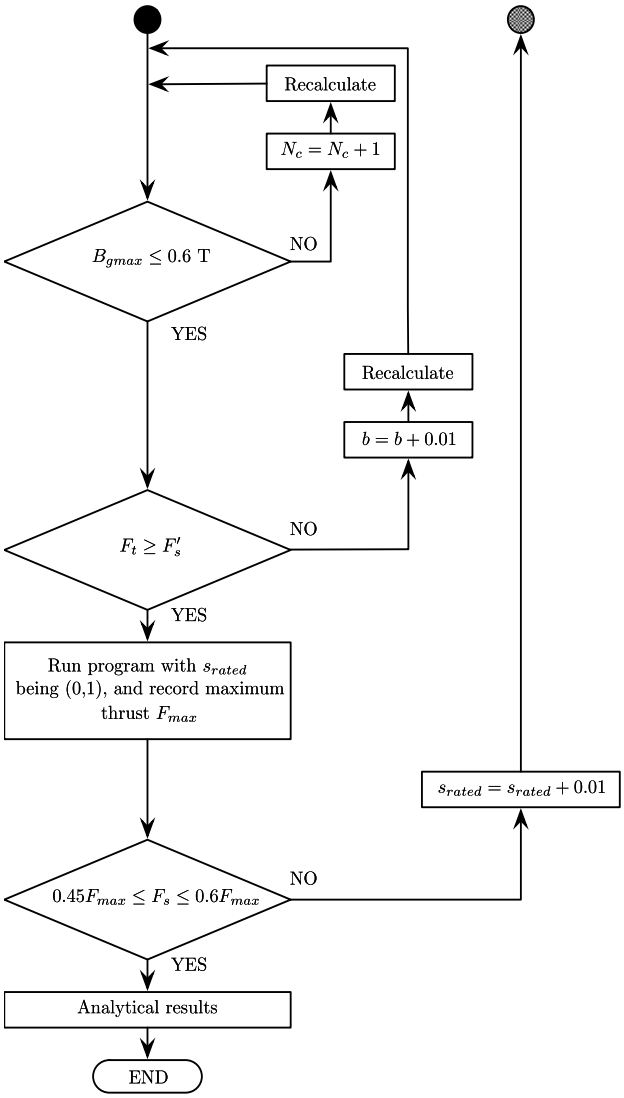

Fig. 4: Flow chart of analytical design, part 2/2.

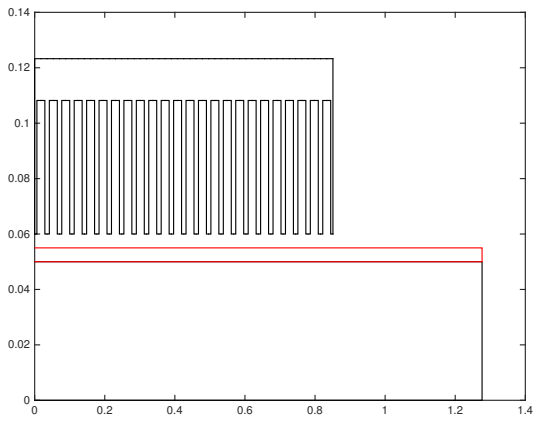

Fig. 5: Preliminary geometry of 8-pole SLIM.

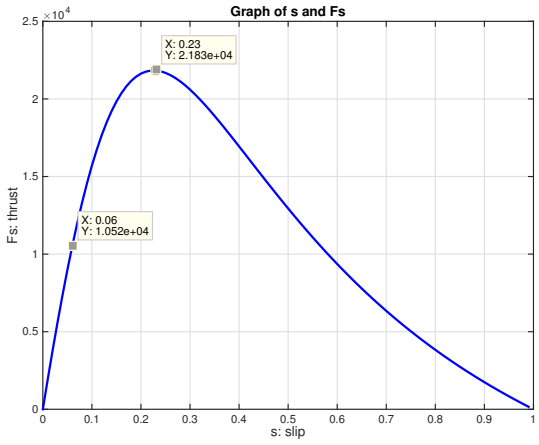

Fig. 6: Thrust to slip curve of 8-pole SLIM.

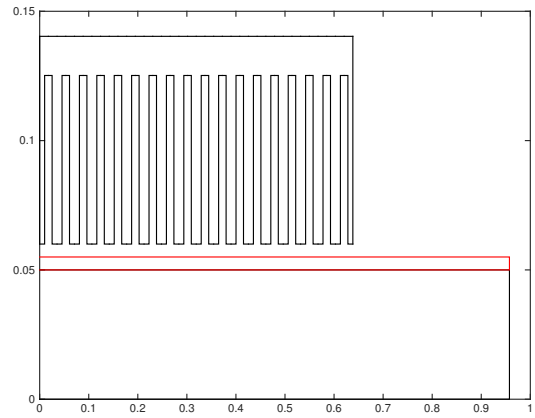

Fig. 7: Preliminary geometry of 6-pole SLIM.

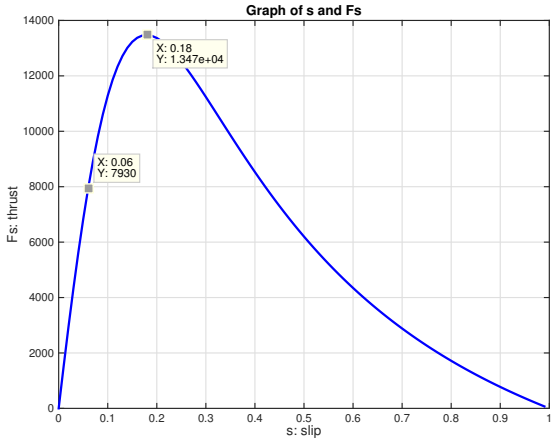

Fig. 8: Thrust to slip curve of 6-pole SLIM.

III. FEM Simulation and Optimization

Since previous experience showed that the result of the analytical model cannot be relied to a large extent [8], the numerical method has to be used for more accurate analysis. Assuming the magnetic field over the SLIM width to be constant and neglecting the edge effect, two-dimensional finite element method (2D-FEM) analysis, carried out in Flux2D software, is employed to testify the validity of the analytical results.

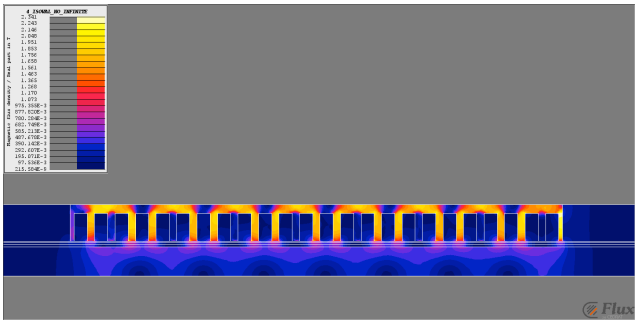

Fig. 9: Flux density distribution of the 8-pole SLIM from the analytical results.

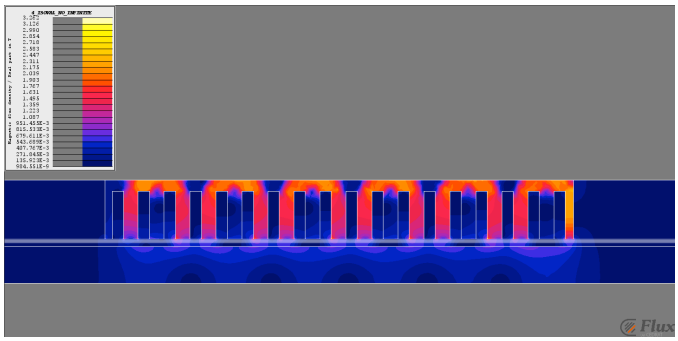

Fig. 10: Flux density distribution of the 6-pole SLIM from the analytical results.

It can be observed from Figs. 9 and 10 that both designs have severe issues of iron saturation in the yoke and teeth as well as the excessive value of B_{gmax} (actual value), which causes the big error, especially in the primary phase current I_1 and in the power factor $\cos\phi$, between the analytical results and FEM analysis results shown in TABLE I and II.

In order to eliminate the iron saturation in the yoke and teeth, and the excessive flux density in the air gap (the actual value of B_{gmax} for the 8-pole and 6-pole SLIM are 0.873 T and 0.797 T, respectively), major parameters of the SLIM: N_c, W_s, b, h_y (height of yoke) and s_{rated}, are marginally modified based on the simulation model. The design scenarios for the 8-pole SLIM are concluded in Figs. 11 and 12 where each dot represents one design solution according to different modification. The plots are sectioned, by the vertical and horizontal dashed lines that are given by the limits, into four areas. It can be observed that only the designs represented by the dots located in the third quadrant of both plots meet the requirements of $F_s' \leq F_t$, actual value of $B_{gmax} \leq 0.6\,T$, $B_{tmax} \leq 1.6\,T$, $B_{ymax} \leq 1.3\,T$, and thereby they are the qualified designs, shown in red color, named as design #1, #2, and #3. With design #3, using the least weight of the primary among these three designs, the cost is the lowest and most space can be saved. Additionally, due to the high mechanical clearance of large LIMs, the length of air gap cannot be reduced anymore. However, a closer look at the flux distribution (shown in Figs. 13-15) gives rise to the fact that design #3 has the least leakage flux, and thereby the most useful flux. The reason behind it can be explained with the highest ratio of slot width to slot pitch. On the whole, the conclusion can be drawn that design #3 is the best solution regarding the 8-pole SLIM.

TABLE I: Comparison between analytical and FEM results of 8-pole SLIM

SLIM	**8-pole**		
Symbol (unit)	***Anal.***	***FEM***	***Error***
F_s (N)	10518	11291	+6.8%
I_1 (A)	656	1086	+39.6%
η (-)	87.2%	77.9%	-12.0%
$\cos\phi$ (-)	0.279	0.202	-37.6%
$\eta\cos\phi$ (-)	0.243	0.158	-54.1%
B_{gmax} (T) (Fundamental value)	0.579	0.625	+7.4%

TABLE II: Comparison between analytical and FEM results of 6-pole SLIM

SLIM	**6-pole**		
Symbol (unit)	***Anal.***	***FEM***	***Error***
F_s (N)	7930	8520	+6.9%
I_1 (A)	522	772	+32.4%
η (-)	87.8%	81.6%	-7.6%
$\cos\phi$ (-)	0.262	0.205	-28.0%
$\eta\cos\phi$ (-)	0.230	0.167	-37.7%
B_{gmax} (T) (Fundamental value)	0.581	0.638	+7.0%

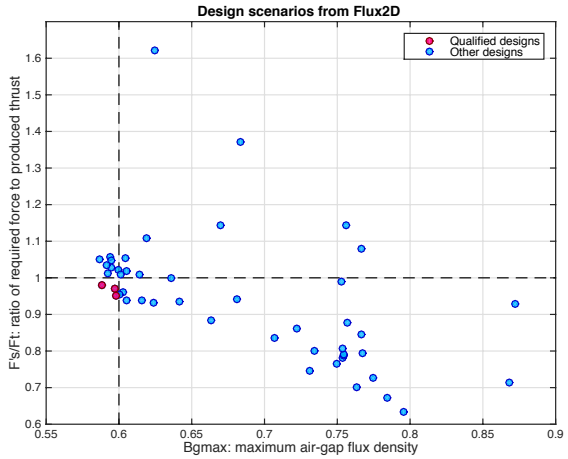

Fig. 11: Design scenarios of 8-pole SLIMs regarding maximum air-gap flux density and force ratio.

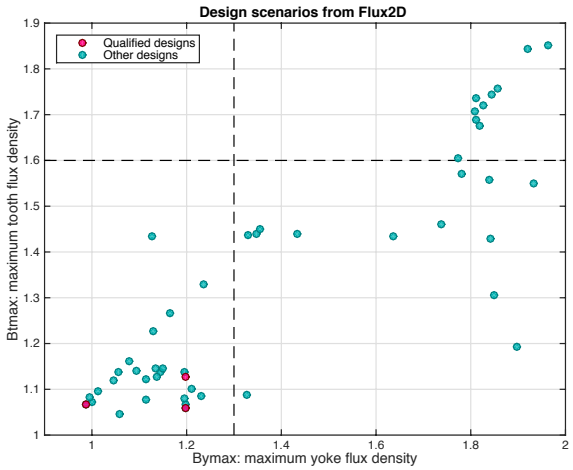

Fig. 12: Design scenarios of 8-pole SLIMs regarding maximum flux density in the yoke and tooth.

The same procedure can be adapted to obtain the optimized results for a 6-pole SLIM. The results of these 30 design scenarios are concluded in two scatter plots shown in Figs. 16 and 17, with identical selection criteria properly set. The qualified 6-pole SLIM designs are indicated as design #4 and design #5, represented by the red dots in the plots. It is noted that with the 6-pole SLIM, three primary units can be applied to propel each pod, in contrast to two primary units with the 8-pole SLIM, restricted by the size of the pod. For the same reason mentioned as 8-pole SLIM, design #5 provides a more efficient solution regarding 6-pole SLIM.

Lastly, the comparison is made between design #3 (8-pole SLIM) and design #5 (6-pole SLIM). Since design #3 has a greater primary core length, the static end effect is thus lower. In addition to that, the power density of design #3 (3.5109 MW/m^3) is larger than that of design #5 (2.5982 MW/m^3). Therefore, design #3 is capable of delivering more power per unit volume. With all aspects considered, the final solution is chosen to be design #3.

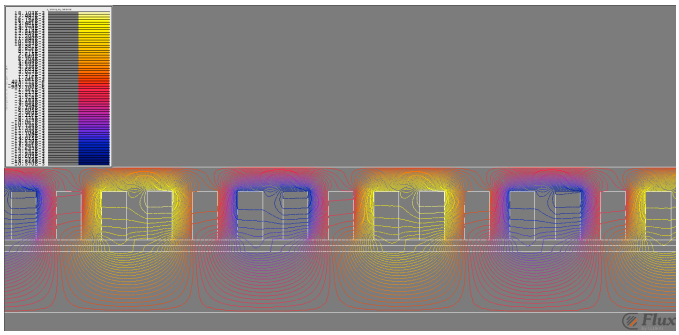

Fig. 13: Flux distribution of design #1.

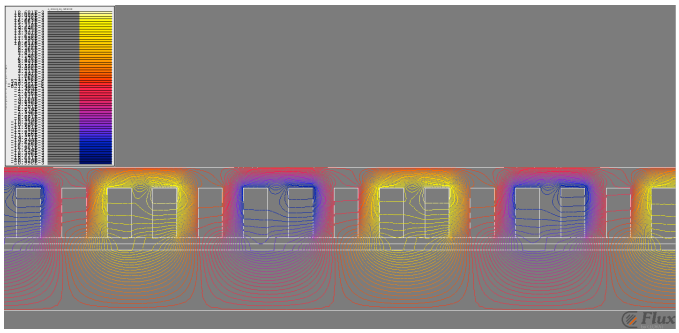

Fig. 14: Flux distribution of design #2.

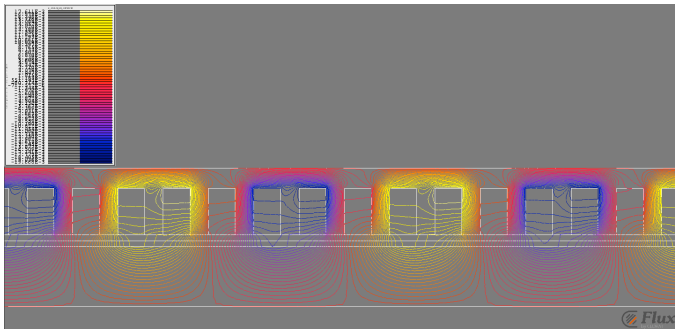

Fig. 15: Flux distribution of design #3.

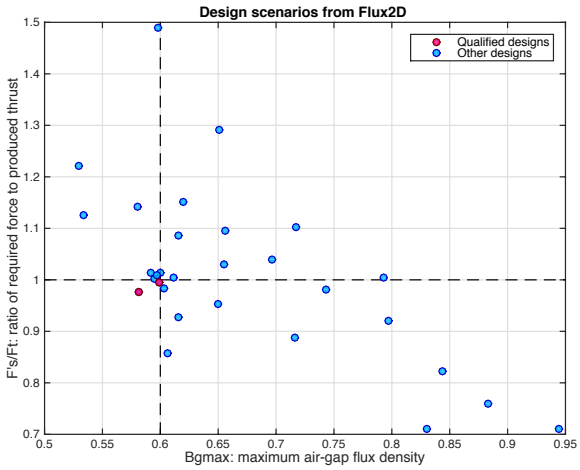

Fig. 16: Design scenarios of 6-pole SLIMs regarding maximum air-gap flux density and force ratio.

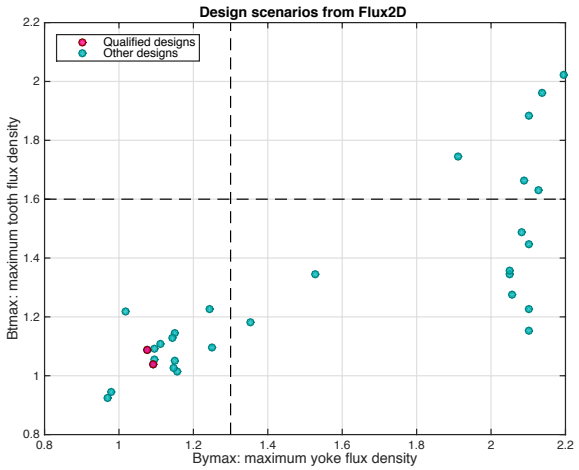

Fig. 17: Design scenarios of 6-pole SLIMs regarding maximum flux density in the yoke and tooth.

The characteristics of the final solution, including thrust, primary phase current, flux density in the air gap, flux density in the tooth, and flux density in the yoke at rated slip, are shown in Figs. 18-21.

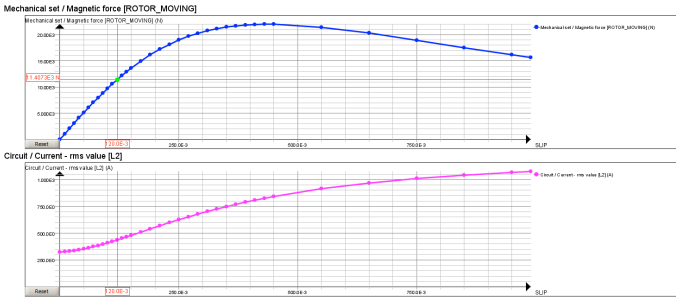

Fig. 18: Thrust and primary phase current versus slip of design #3.

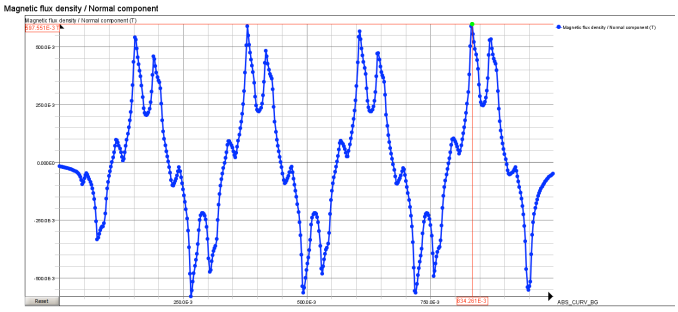

Fig. 19: Flux density in the air gap at the rated slip of 0.12 of design #3.

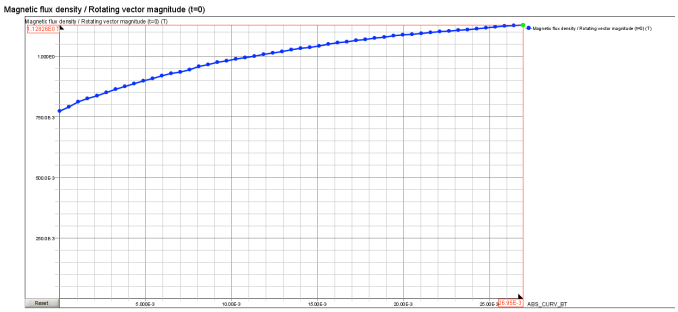

Fig. 20: Flux density in the tooth at the rated slip of 0.12 of design #3.

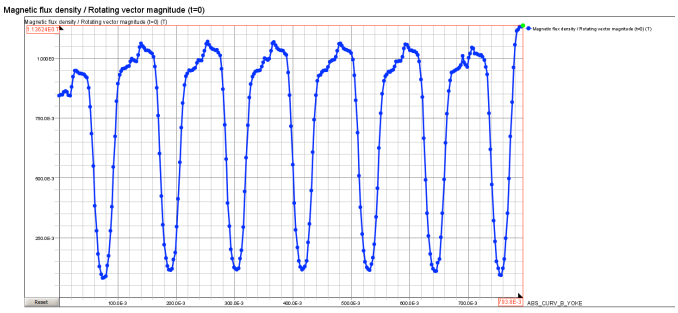

Fig. 21: Flux density in the yoke at the rated slip of 0.12 of design #3.

The comparison between the results of the analytical model and the FEM analysis of design #3 is made as a reference, shown in TABLE III. In addition to meeting the requirements stated above and eliminating the iron saturation, all the errors have been reduced to acceptable values that validate the accuracy of the analytical model.

IV. Conclusion

The analytical model is designed, based on which the characteristics and preliminary geometry are derived. The issue of iron saturation and big errors are eliminated and diminished by modifying the simulation model. The optimized design solution is obtained in terms of power density, flux leakage and end effect. The articulated funiculator is capable of vertically rising with all the requirements met by using the final design solution of two 8-pole SLIMs propelling for a single pod.

ACKNOWLEDGMENT

The authors would like to acknowledge Mr. Fritz King at Tyréns AB for collaborating on the project. Thanks also goes to Associate Professor Oskar Wallmark at KTH for his support and help in the thesis work, and to Associate Professor Juliette Soulard at KTH and Dr. Patrick Lombard at CEDRAT for helping to solve problems regarding the Flux2D software.

REFERENCES

[1] J. F. Gieras, Linear Induction Drives. New York: Oxford University Press Inc, 1994.

[2] I. Boldea and S. A. Nasar, The Induction Machine Handbook. CRC Press, 2002.

[3] M. S. Manna, S. Marwaha, and C. Vasudeva, "Accuracy assesment of the linear induction motor performance using adaptive FEM," COMSOL Conference. Bangalore, 2009.

[4] M. S. Manna, S. Khajuria, and S. Marwaha, "Thrust analysis and improvement of single sided linear induction motor using finite element technique," International Press Corporation, vol. 3, no. 2, June 2013.

[5] F. King, M. Lundström, S. Salovaara, and P. Severin, "Articulated funiculator and the tubed mega frame," Council on Tall Buildings and Urban Habitat. Shanghai, pp. 563, 2012.

[6] A. H. Isfahani, B. M. Ebrahimi, and H. Lesani, "Design optimization of a low-speed single-sided linear induction motor for improved efficiency and power factor," IEEE Transactions on Magnetics, vol. 44, no. 2, Feb. 2008.

[7] S. A. Nasar and I. Boldea, Linear Motion Electric Machines. John Wiley and Sons, Inc., 1976.

[8] W. M. Arshad, "A low-leakage linear transverse-flux machine for a free-piston generator," Ph.D. dissertation, KTH-Royal Institue of Technology, 2003.

Table III: Comparison between analytical and FEM results of the optimized design of SLIM

SLIM	**The optimal design (#3)**		
Symbol (unit)	***Anal.***	***FEM***	***Error***
F_s (N)	11275	11407	+1.2%
I_1 (A)	401	438	+8.3%
η (-)	82.8%	81.2%	-2.0%
$\cos\phi$ (-)	0.514	0.486	-5.7%
$\eta\cos\phi$ (-)	0.426	0.395	-7.8%
B_{gmax} (T) (Fundamental value)	0.363	0.382	+5.0%